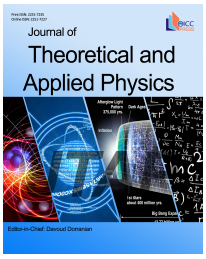

Volume 19, Issue 1, 192511 (1-10)

Journal of Theoretical and Applied Physics (JTAP)

https://doi.org/10.57647/j.jtap.2025.1901.11

The effect of nitrogen ion implantation on electrical impedance and corrosion resistance of aluminum

Fatemeh Abdi*

Department of Engineering Sciences, Faculty of Advanced Technologies, University of Mohaghegh Ardabili, Namin, Iran.

***Corresponding authors:** f.abdi@uma.ac.ir

Original Research

Received:
9 November 2024
Revised:
24 December 2024
Accepted:
13 January 2025
Published online:
10 February 2025

© 2025 The Author(s). Published by the OICC Press under the terms of the Creative Commons Attribution License, which permits use, distribution and reproduction in any medium, provided the original work is properly cited.

Abstract:

In this work, in order to investigate the effect of implantation temperature on the corrosion resistance of the sample, nitrogen ions with energy of 30 keV were implanted on the aluminum substrate at different implantation temperatures. The thickness of created aluminum nitride, surface morphology and intensity of nitride and oxide phases were investigated by means of XPS, AFM and XRD respectively. The results showed that the intensity of the oxide and nitride phases depend on the implantation temperature and as the intensity of the oxide phases increases, the intensity of the nitride phases decreases. Also, the results showed that there is a critical temperature where the intensity of the nitride phase is minimum and the surface has the smallest grains. To investigate the effect of implantation temperature on corrosion resistance, polarization and EIS tests were performed. The results showed that at the critical temperature, the corrosion current is maximum. By simulating the equivalent circuit, the cause of low corrosion resistance at this temperature was investigated and attributed to the low electrical impedance. Finally, the surface of the corroded samples was observed by electron microscopy.

Keywords: Aluminum; Ion implantation; Corrosion resistance; EIS; Equivalent circuit

1. Introduction

According to the principles of the corrosion process, when a substance is placed in a corrosive environment, it loses electrons and is corroded. The faster the electron loss, the faster the corrosion. Therefore, to control the corrosion rate, the rate of electron loss must be controlled. In other words, to increase corrosion resistance of the sample, the electrical impedance of it must be increased. Due to the fact that electrical impedance depends on elements such as electrical resistance, capacitance and inductance, by increasing the electrical resistance, reducing the capacitance and inductance, electrical impedance and corrosion resistance can be increased. Due to the fact that these elements depend on the material type and material geometry, the corrosion resistance can be increased by changing the type and geometry of the material [1–5].

The use of coating methods such as polymer coating [6–10], physical vapor deposition (PVD) and chemical vapor deposition (CVD) [11–15] is the methods that has been done with different materials on different metals. In these methods, by creating a protective layer on the metal, the electrical impedance increases. In these methods, due to the fact that a substance is placed on the metal, the dimensions of sample change.

One of the methods to increase the electrical impedance without changing the dimensions of the material is the method of implanting ions on the metal surface. In this method, the properties of the material do not change in bulk dimensions. The penetration depth of ions is between 0.01 µm to 1 µm. Ion implantation has other advantages, such as low working temperature and reproducibility. Studies have shown that ions such as nitrogen are very efficient ion in the implanting process [16–21].

In the implantation process, the presence of another material is not the only reason for changing the corrosion resistance, but with ion implantation, the crystalline property, grain distribution (surface morphology) also changes. By changing the electrical resistance and capacitance, the corrosion resistance changes [22].

Aluminum is widely used in industry due to its lightness [23], high conductivity and good corrosion resistance (due to the formation of an oxide layer on its surface) [24, 25]. However, this widely used material is vulnerable in the presence of corrosive ions, such as chlorine, due to the breaking of the oxide layer, and increasing its corrosion resistance is a necessity [26–28]. So far, there have been many reports

of the use of nitrogen ion implants to increase corrosion resistance. The reason for using nitrogen ion implants to protect against corrosion is the high solubility of this ion in Aluminum. Ion implantation increases corrosion resistance by microstructural changes, the creation of new phases, and changes in chemical and mechanical properties. Aluminum nitride, in addition to increasing the corrosion resistance of aluminum, is very important due to its hardness, electrical properties (energy gap of 6.3 electron volts) and high melting point [22].

Researchers have used ion implantation to study the corrosion protection of various aluminum alloys [16–21]. Most studies have been performed on 6000 series alloy. Investigation of ion implantation for corrosion protection of 7000 series, showed that nitrogen ion implantation does not have much effect on increasing corrosion resistance due to the presence of Zn element which is a sacrificial substance [19]. In our previous work, by implanting nitrogen ions of different energies on the surface of aluminum, we showed that the corrosion resistance of 7049 series aluminum can be increased [26]. Due to the fact that using ion implantation at different temperatures can change the surface material and surface morphology, in this work by implanting nitrogen ions at different temperatures on the aluminum 7049 sample, electrical impedance has been investigated.

2. Experiment

Aluminum samples with dimensions of 20 mm $\times$ 20 mm $\times$ 3 mm were first cleaned in acetone and then in alcohol, in an ultrasonic bath. Table 1 shows the X-ray fluorescence (XRF) results of aluminum sample and its compounds. For implantation, aluminum samples were placed in the substrate holder in a vacuum chamber, while their temperature was controlled by a thermocouple inside the retaining cavity of the substrate. The details of this work have been reported in our previous works [26, 27].

The base pressure for ion implantation was 2×10^{-5} mbar. Nitrogen ion implantation with flux of 5×10^{17} ion/cm^2 performed on aluminum samples at 30 keV and different temperatures of 300 K, 400 K, 500 K and 600 K, for 1800 s.

In the ion implantation process, the ion current density was set to 44 A/cm^2. During the ion implantation process, the chamber pressure increased to 5×10^{-5} mbar. Surface element analysis was performed by X-ray photoelectron spectroscopy (XPS). The crystal structure of the samples was examined using X-ray diffraction pattern (XRD) with a step of 0.01° and a time constant of 1 s, and the morphology of ion implanted samples was examined using an atomic force microscope (AFM). Polarization test was performed to evaluate the corrosion rate and corrosion tendency and EIS test measurement used to evaluate the corrosion resistance of ion implanted layers with different temperatures. The electrochemical test of the samples was performed using potentiodynamic method with a potentiostat coupled to PC (273A, EG & G, USA). Electrochemical impedance spectroscopy (EIS) was performed using a potentiostat coupled to PC (Ivium, De Zaale 11, 5612 AJ Eindhoven, Netherlands) with reference to the open circuit potential (OCP). 3.5% NaCl solution was considered as corrosive solution and AgCl solution, reference electrode and platinum electrode were used as auxiliary electrode.

The samples were placed in the fixture as a working electrode in such a way that only a circle with a diameter of 1 cm of the samples was exposed to the corrosive environment. Polarization test was measured with potential starting from -0.5 V to 0.5 V with a speed of 50 mV/s and EIS measurements were performed in the frequency range of 100000 Hz to 0.01 Hz and with a voltage amplitude of 0.01 V. Prior to measurement, the samples were immersed in NaCl solution for 0.5 h to stabilize the OCP potential. After corrosion testing, SEM images were taken from the samples to observe the surface.

3. Results

3.1 SRIM and XPS results

The distribution of N^+ ions implanted in aluminum samples with 30 keV energy was simulated using SRIM 2000. The mean distance of the implanted ions from the surface (projected range) denoted by Rp and the deviation from this value due to different ion energies (straggle range) and denoted by $\Delta R_{L_{1,2}}$ are given in Table 2 (L_1 and L_2 indicates longitudinal and transverse deviations). It should be noted that the effect of temperature, particle flux and parameters such as surface roughness, etc. are not included in SRIM2000 calculations. This simulation shows that the maximum penetration depth of ions is about 70 nm.

Due to the fact that the used aluminum sample contains various elements, and because ion implantation occurs on the surface of the sample, also due to the presence of an oxide layer on the surface of aluminum (which is considered as a protective layer), the XPS (X-Ray photoelectron spectroscopy) analysis was performed. The results of this analysis are shown in figures 1 (a) and (b), for non- implanted and ion implanted samples respectively, at 30 keV energy and 300 K temperature. From figure 1 (a), it is clear that the percentage of Zn, Mg and Cu elements is very low, so they are not effective in the formation of the oxide phase to protect the aluminum. So, the layer that is formed to protect the 7049 aluminum sample is the aluminum oxide layer. It is clear from the figure that there is a layer of aluminum oxide close to the surface (4

Table 1. Chemical composition of aluminum ALLOY 7049 given from XRF analysis.

Element (wt%)														
Al	Zn	Mg	Cr	Cu	Si	Fe	S	Cl	K	Ca	Mn	P	Ga	Ti
83.3	8.2	4.1	0.31	2.1	0.23	0.22	0.10	0.035	0.017	0.029	0.040	0.014	0.015	0.050

Table 2. Results of SRIM simulation.

T (K)	Rp (nm)	ΔRp_{L1} (nm)	ΔRp_{L2} (nm)
300	70	30	24

nm). Figure 1 (b) shows that for the implanted sample, the nitride layer is formed at a greater depth of the surface. In other words, the thickness of the nitride layer is greater than the thickness of the oxide layer. Due to the fact that distribution of ions was Gaussian, This figure shows that the highest intensity of the nitride phase is formed at a depth of about 60 nm.

3.2 XRD results

XRD result of the aluminum sample is shown in figure 2. It is clear from the figure that the aluminum spectrum has 6 XRD peaks which correspond to the Al (111), Al (200), Al (220), Al (311), Al (222) and Al (400) crystalline plates are located in $2\theta = 38.43°$, $2\theta = 44.68°$, $2\theta = 65.03°$, $2\theta = 78.14°$, $2\theta = 82.35°$ and $2\theta = 98.98°$ respectively (Standard Card No. 1327-85). There is also another peak in the $2\theta = 41.50°$ which indicates the phase of Al_2O_3 (123) (Standard card number 88-0107). The diffraction pattern of ion implanted aluminum samples with 30 keV energy at different temperatures and its comparison with the diffraction pattern of aluminum specimen is shown in figure 3. The results show that the effect of nitrogen ion implantation in aluminum the intensity of the aluminum peaks decreases, but secondary peaks are seen near the aluminum peaks indicating the formation of an aluminum nitride phase. These peaks are located in $2\theta = 44.8°$, $2\theta = 65.2°$, $2\theta = 78.39°$, $2\theta = 82.6°$ and $2\theta = 99.31°$ which correspond to the crystalline plates of AlN (200), AlN (220), AlN (311), AlN(222) and AlN (400) respectively (Standard Card No. 46–1200). In addition to the formation of the aluminum nitride (AlN) phase, the XRD spectrum also shows the formation of the aluminum oxide (Al_2O_3) and zinc nitride (Zn_3N_2) phases. The XRD peaks at the $2\theta = 19.66°$, $2\theta = 41.40°$, $2\theta = 40.72°$, $2\theta = 20.84°$ and $2\theta = 42.38°$ represent the phase Al_2O_3 (101), Al_2O_3 (302), Al_2O_3 (116), Al_2O_3 (202) and Al_2O_3 (404) respectively according to the standard card (88–0107, 73–1199, 71–1684, 210010 and 02–1227, respectively) and the peak of $2\theta = 22.34°$ indicate formation of Zn_3N_2 (211) (Standard Card No. 88–0618).

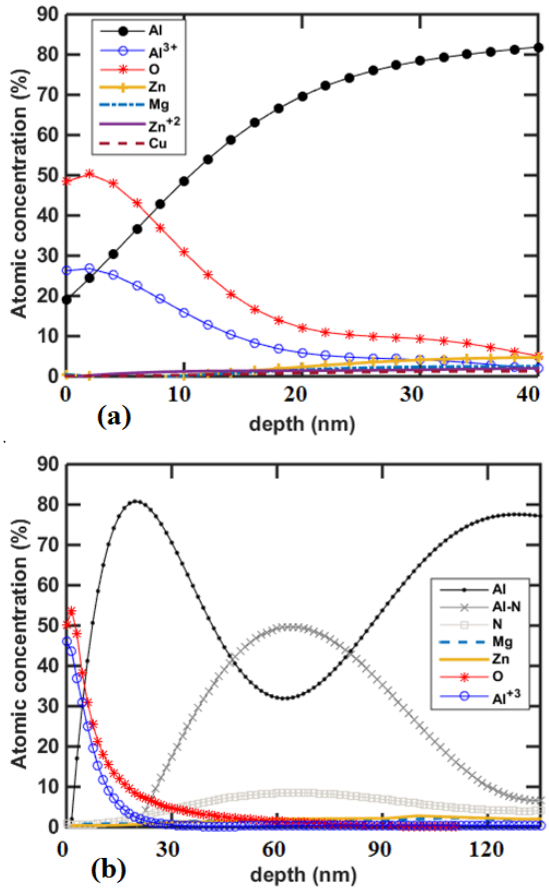

Figure 1. XPS depth profile of (a) non implanted aluminium and (b) implanted aluminium.

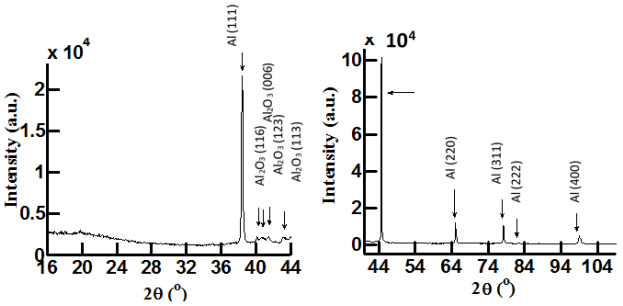

Figure 2. XRD spectrum of aluminum.

The change in intensity of different phases of aluminum nitride and aluminum oxide with temperature are shown in Table 3. The results show that there is a critical temperature in the nitrogen ion implantation process in which the intensity of the nitride phase decreases. The reason for this minimum was attributed to the presence of residual gases. In fact, the gases remaining in the chamber, and the decomposition of water that occurs at high temperatures, produce oxygen, and the resulting oxygen can easily react with the sample surface to form an oxide layer. Due to the fact that the oxide layer is more stable than the nitride layer at high temperatures, with increasing temperature, the intensity of the oxide phase increases. As the temperature rises further and there is extra energy, the oxygen molecules leave the surface again and the conditions for AlN formation are provided again. The presence of minimum in nitride phase intensity in the nitrogen ion implantation process at different temperatures has already been reported [28].

3.3 AFM results

Figure 4 shows the surface of the aluminum sample. The surface morphology of ion implanted samples with different temperatures is shown in figure 5. It is clear from the figures that all the implanted samples have smaller grains than the aluminum sample due to the sputtering effect. It is clear from figure 5 (a) that the sample implanted at 300 K temperature has a dome-shaped structure and at a temperature

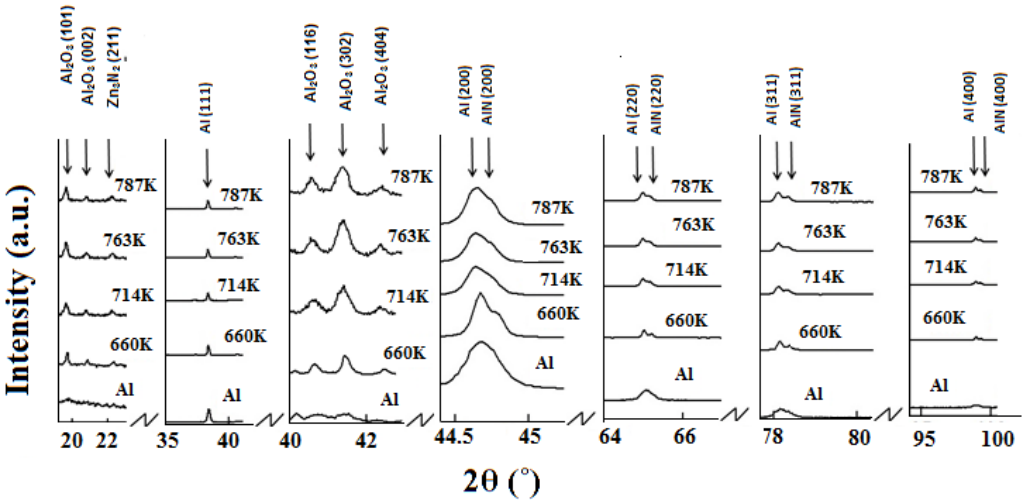

Figure 3. XRD spectrum of implanted aluminum at different temperatures.

of 400 K this structure becomes a pointed conical structure. It is clear from figure 5 (b) that at this temperature, fine grains were distributed among the coarse grains. It is also known that the ion implanted sample at this temperature has smaller grains than the implanted sample at 300 K. Figure 5 (c) shows that the ion implanted sample at 500 K temperature has a sharper structure and smaller grains than the ion implanted samples at 300 K and 400 K temperatures.

This is due to the penetration of nitrogen ions into the grains and break the grains into fine grains. Figure 5 (d) shows that as the implanted temperature increases to 600 K, the grain size increases again due to the increase in the diffusion phenomenon.

The average grain size (D), average roughness (R_{ave}) and deviation from the average (R_{rms}) have obtained using WSXM software for ion implantation samples at different temperatures. These results are shown in Table 4. The results show that the sample implanted at 500 K temperature has the smallest grain size and the lowest roughness among all samples.

3.4 Corrosion results

To evaluate the corrosion rate of the samples, polarization test was performed on the samples. Figure 6 shows the results of this test. Table 4 shows the corrosion current density and corrosion potentials obtained from the figure for different samples. It is clear from the results that the corrosion current decreases due to ion implantation and the corrosion potential increases. This is because of the nitride phase's formation.

In the study of the temperature effects on corrosion resistance, it was found that by increasing the temperature from 300 K to 500 K, the corrosion current increases and the corrosion potential decreases due to the reduction of nitride phase intensity and reduction of grain size. With increasing temperature to 600 K, due to increasing of nitride phase intensity and increasing grain size, corrosion current decreases and corrosion potential increases. The corrosion current and corrosion potential of different samples are shown in figure 7.

For more investigations, EIS test was performed. Figure 8 shows the results of this test. It is clear from the results that with increasing the temperature from 300 K to 500 K, the corrosion resistance decreases and with increasing the implanted temperature to 600 K, the corrosion resistance increases. To better investigate and calculate the electrical impedance and its effect on the corrosion resistance, the equivalent circuit of samples was obtained and studied.

Figure 9 shows the equivalent circuit of implanted samples at different temperatures. In this circuit, *Rs* is the electrical resistance of the solution. It is clear from the figure that the equivalent circuit of an aluminum sample in a corrosive solution has a capacitance, which is the double layer capacitance and is due to the presence of an oxide layer on

Table 3. Intensity changes of AlN and Al_2O_3 with temperature.

Temoerature (K)	Intensity (a.u.)								
	AlN				Al_2O_3				
	(200)	(220)	(311)	(400)	(101)	(116)	(002)	(302)	(404)
300	7000	830	780	400	3	2	0.5	10	1
400	3900	750	590	450	5	15	1	60	5
500	2500	690	520	300	6	20	1.5	100	15
600	8200	1050	800	900	4	14	1	60	10

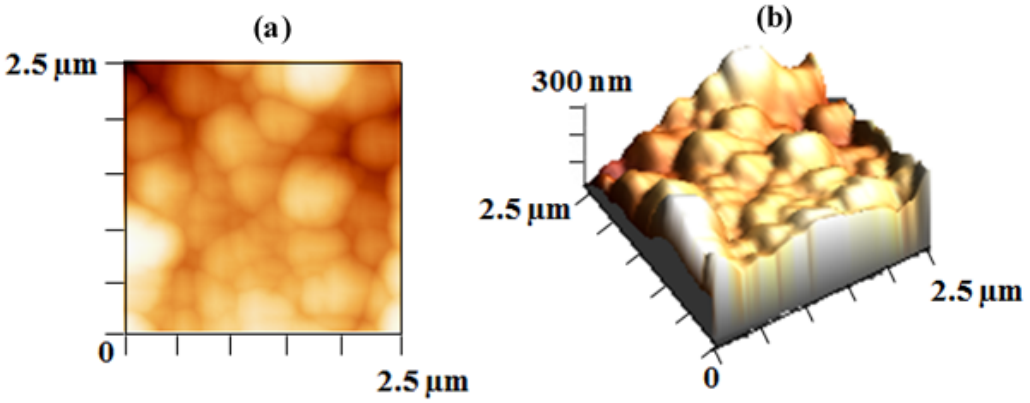

Figure 4. AFM images of non-implanted aluminum.

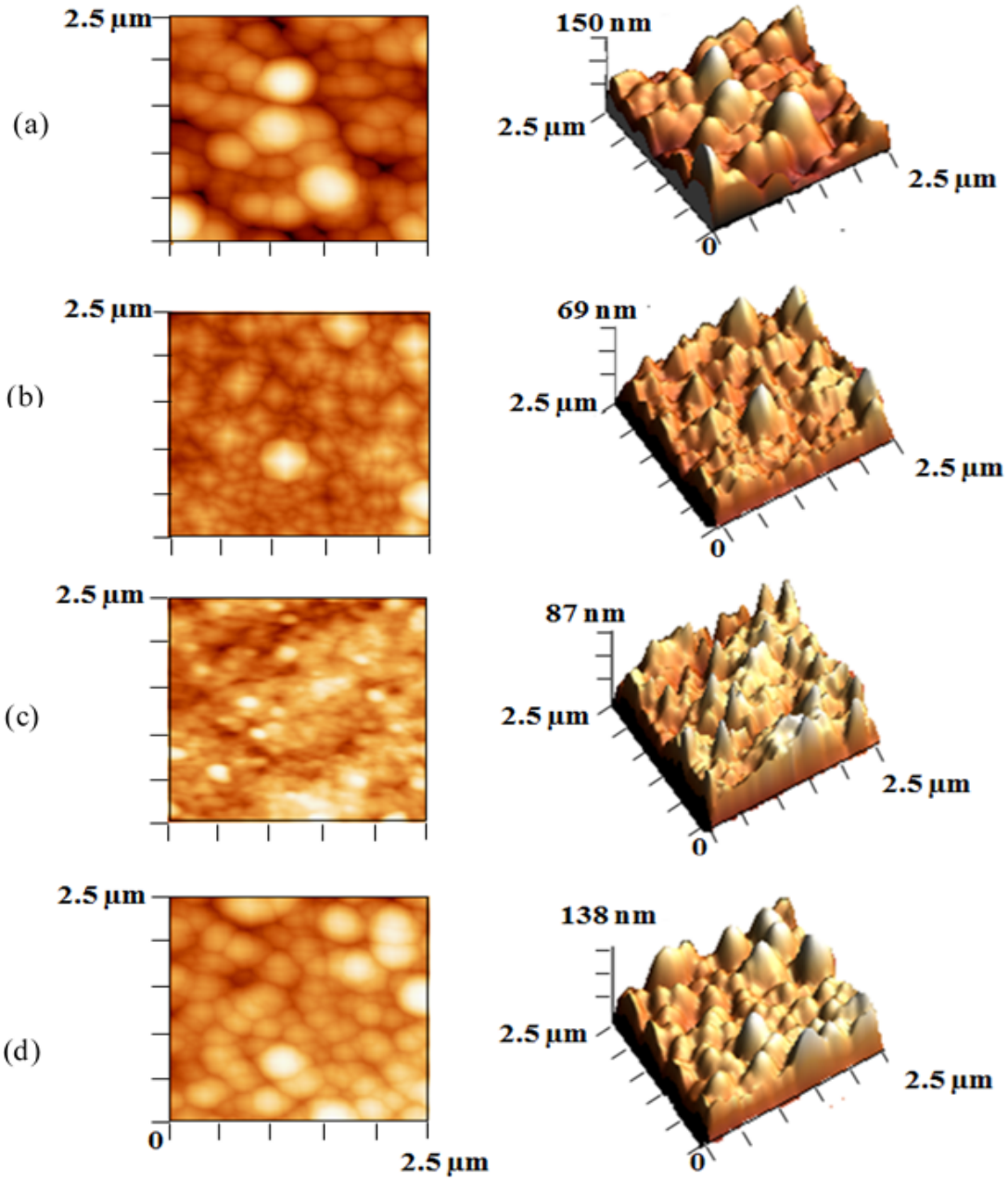

Figure 5. AFM images of implanted aluminum at different temperatures of (a) 300 K, (b) 400 K, (c) 500 K, (d) 600 K.

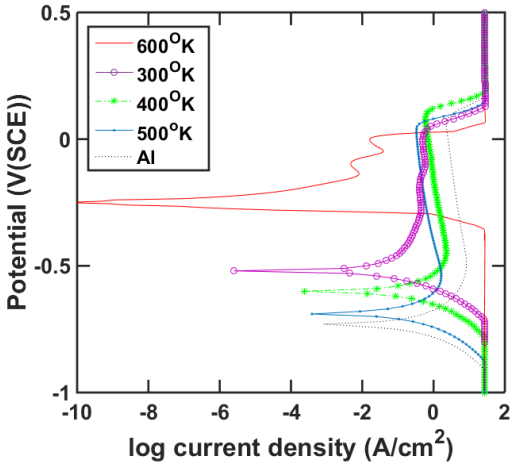

Figure 6. Polarization test results of non-implanted aluminum and implanted aluminum at different temperatures.

aluminum. This sample also has inductance behavior. This inductance behavior is due to the breaking of the aluminum oxide layer by chlorine ions and the penetration of ions into the sample. The results show that the inductance behavior of the aluminum sample is eliminated by implantation. The equivalent circuit of implanted samples consists of two capacitances, one of which is the double layer capacitance and the other is the coating capacitance, which is due to the formation of the nitride phase. As mentioned before, the coating capacitance is much smaller than the double layer capacitance and can be seen at higher frequencies. It is well known that, the greater the number of grains, (large grains) the larger the capacitance.

EIS results show that by increasing the implantation temperature from 300 K to 500 K, the electrical impedance decreases thus the corrosion resistance decreases. As XRD images showed, by increasing the implanted temperature from 300 K to 500 K, the intensity of the nitride phase decreases and the intensity of the oxide phase increases.

The XPS results showed that the nitride phase was deeper than the oxide phase. In other words, the thickness of the nitride layer was much greater than the thickness of the oxide layer. Therefore, according to the equation (1) (where d is the thickness of the coating and k is the dielectric constant of the coating) and given that the dielectric constant of the oxide and nitride phases is close to each other ($k = 9$), the double layer capacitance of the oxide layer is higher than the double layer capacitance of the nitride coating. So its electrical impedance is smaller, which is one of the factors reducing corrosion resistance of the sample implanted at 500 K temperature.

$$C = k\varepsilon_0 \frac{A}{d} \tag{1}$$

AFM results also showed that as the temperature increased from 300 K to 500 K, the grain size became smaller and the number of grain boundaries increased. As the number of grain boundaries increases, the capacitance of the coating increases. Because this capacitance is the result of a large number of parallel capacitances and with increasing the number of grain boundaries (increasing the number of parallel capacitances), the total capacity increases, so

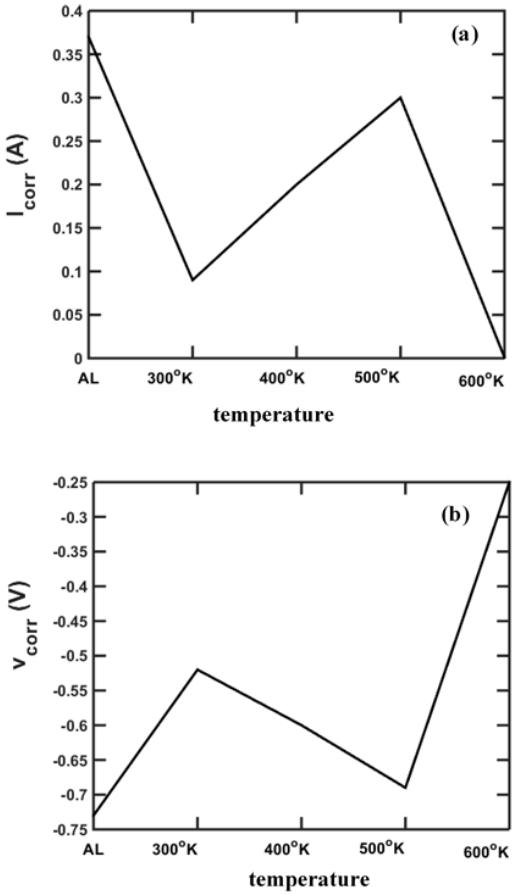

Figure 7. (a) Corrosion current and (b) Corrosion potential of non-implanted aluminum and implanted aluminum at different temperatures.

Table 4. AFM and polarization tests result of the samples implanted at different temperatures.

sample	Al	300 K	400 K	500 K	600 K
Grain Size (nm)	355	309	176	136	273
Average Roughness (nm)	35	16	6	9	15
Rms (nm)	44	20	8	11	19
Vcorr (V)	−73	−0.52	−0.6	−0.69	−0.25
Icor	37×10^{-2}	9×10^{-2}	20×10^{-2}	30×10^{-2}	9×10^{-4}

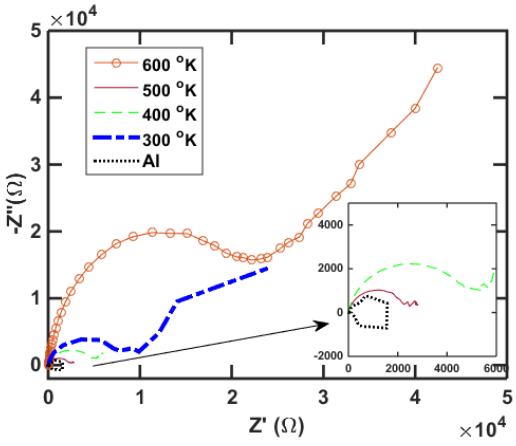

Figure 8. EIS results of non-implanted aluminum and implanted aluminum at different temperatures.

the capacitance of the coating increases and the electrical impedance decreases. This is another factor to reduce corrosion resistance at 500 K. Therefore, due to the decrease in electrical resistance (decrease in nitride phase intensity), increase in double layer capacitance (less oxide layer thickness compared to nitride coating) and increase in capacitance of coating (small grains) at 500 K implantation temperature, electrical impedance decreases, these leads to decreasing of corrosion resistance at this temperature. Corrosion current decreases with increasing temperature to 600 K due to increased nitride phase intensity, increased grain size, increased electrical resistance, decreased double layer capacitance and decreased coating capacitance.

The fit between the bode and phase diagrams of the EIS test and the equivalent circuit simulation for different samples are shown in figure 10 and figure 11 respectively. This figures show the best fit between the experimental and simulation results. The equivalent circuit quantities obtained from this fit are given in Table 5. In this table, *Rs* is the resistance of soluble and for all samples, is almost constant. Because the area of the sample that is exposed to the corrosive environment is very small compared to the volume of the solution. The results show that for aluminum sample, due to damage of oxide layer in the salt solution,

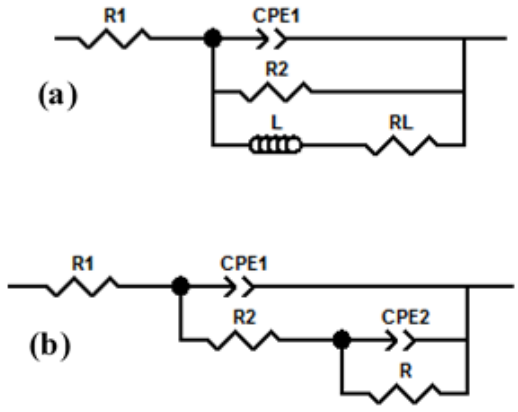

Figure 9. Equivalent circuit of (a) non-implanted aluminum and (b) implanted aluminum at different temperatures.

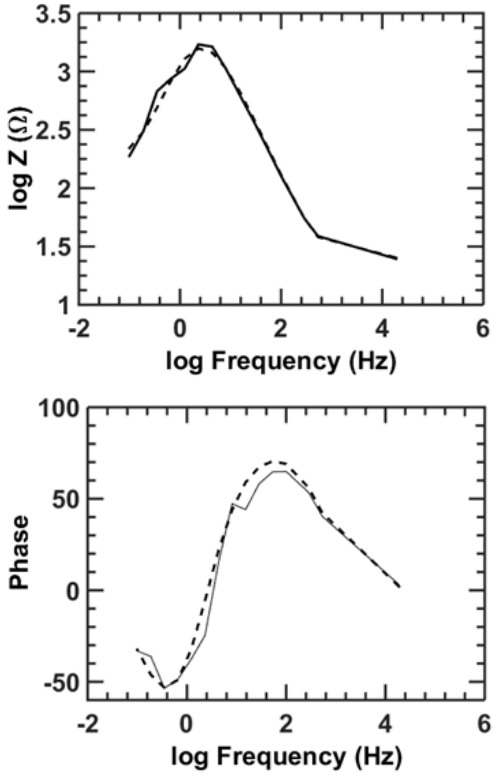

Figure 10. Bode and phase diagram of non-implanted aluminum. Solid line: experimental and Dashed line: simulation.

there is induction behavior (L). The results show that for the implanted samples, due to nitride phase formation and impossibility of chlorination porosity, this induction behavior disappears. It is also clear from the table that with increasing implanting temperature from 300 K to 500 K, the electrical resistance (R) decreases due to the decrease in the intensity of the nitride phase and due to the damage of the oxide layer. It is also clear that due to the increase in oxide intensity and decrease in nitride intensity with increasing temperature from 300 K to 500 K, the capacitance of the double layer (C_d) increases. The reason is the low thickness of the oxide layer compared to the nitride protective layer. It is also known that with increasing temperature from 300 K to 500 K, the capacitance of the coating capacitance (C_{cot}) decreases due to the smaller grain size. As the temperature increases further to 600 K, due to the increase in grain size, the capacitance of the coating decreases and with increasing the intensity of the nitride phase, the electrical resistance increases and the capacitance of the double layer decreases. The α parameter is entered in the calculations because the surfaces of the samples are not smooth. This parameter indicates the amount of surface roughness and is maximum for implanted sample at 500 K, because, as the AFM results showed, this sample has the lowest roughness.

3.5 SEM results

The SEM images of the samples after the corrosion test are shown in figure 12. These images show that implanted samples were less degraded than aluminum sample. As can be seen from the figures, the aluminum sample has a cavity corrosion which is due to the inductance behavior

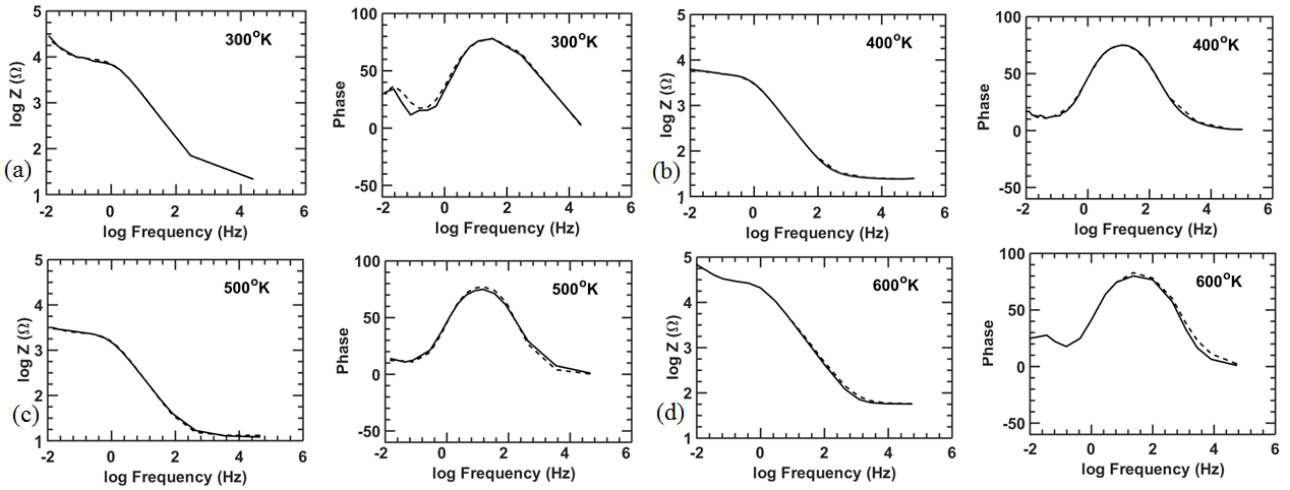

Figure 11. Bode and phase diagram of implanted aluminum at different temperatures of (a) 300 K, (b) 400 K, (c) 500 K, (d) 600 K. Solid line: experimental and Dashed line: simulation.

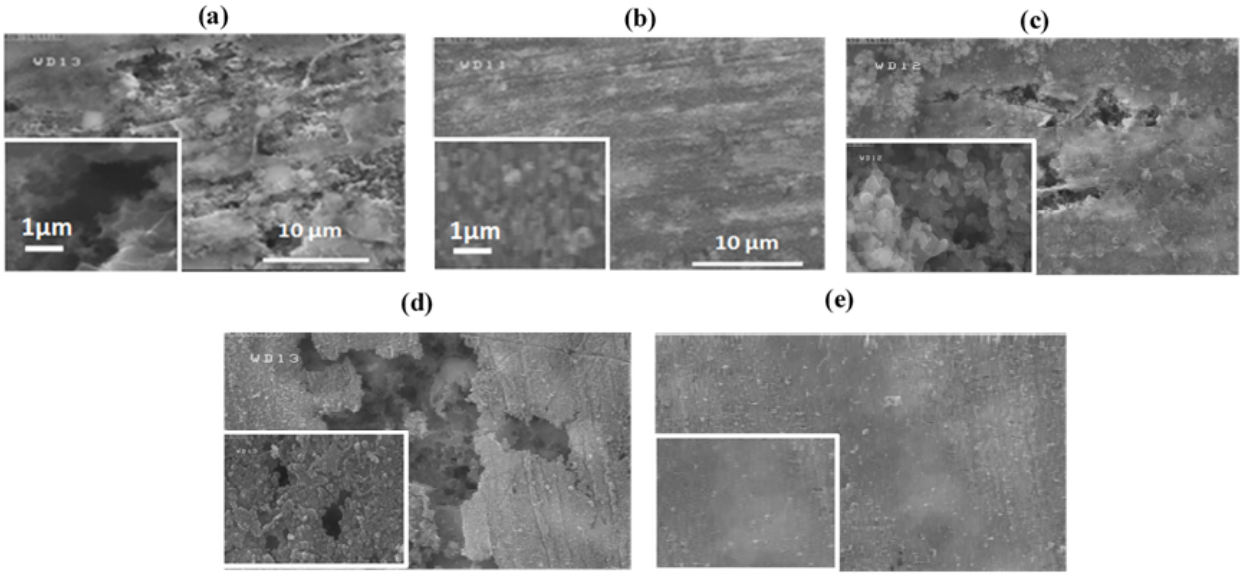

Figure 12. FESEM images of (a) Non implanted aluminum, (b) Implanted aluminum at 300 K, (c) Implanted aluminum at 400 K, (d) Implanted aluminum at 500 K, (e) Implanted aluminum at 600 K.

Table 5. Equivalent circuit parameters for implanted samples at different temperatures.

sample	Al	300 K	400 K	500 K	600 K
Rs (Ω)	25	22	26	22	23
R_1 (Ω)	1660	9370	4960	2350	30108
R_2 (Ω)	-	23400	2642	1524	62307
R_L (Ω)	166	-	-	-	-
C_d (F)	1.93×10^{-5}	5×10^{-4}	38×10^{-4}	99×10^{-4}	3×10^{-4}
C_{cot} (F)	-	1×10^{-5}	38×10^{-6}	76×10^{-6}	6×10^{-6}
α_1	0.91	0.94	0.95	0.97	0.96
α_2	-	0.94	0.95	1	0.96
L (H)	230	-	-	-	-

of the samples which was also seen in the Nyquist curve (as a result of the penetration of chlorine ions and breaking of the oxide protective layer). The results show that for the implanted sample at 300 K, due to the formation of the nitride phase, and increased electrical impedance, the sample surface was less damaged. It is also clear from the figures that by increasing the implanting temperature from 300 K to 500 K, due to the decrease in electrical impedance (decrease in nitride phase intensity (decrease in electrical resistance and increase in double layer capacitance) and decrease in grain size (increase in coating capacitance), corrosion resistance decreases and the sample surface is damaged. Therefore, ion implanted samples at 500 K have the lowest corrosion resistance and the most damage.
SEM images of nitrogen ion implantation samples at 600 K show that due to high electrical impedance, these samples have the highest resistance to corrosion and have the least damage.

4. Conclusion

In this work, nitrogen ions with the energy of 30 keV at different implantation temperatures were implanted on the surface of aluminum substrate. XPS depth profile analysis was used to investigation of aluminum nitride film thickness. Crystal structure and surface morphology of the samples were investigated by means of XRD and AFM, respectively. The results showed that the crystal structure and grain size are strongly dependent on the implantation temperature. It was concluded that with increasing implantation temperature, the intensity of oxide phases increases, the intensity of nitride phase decreases and the grains become smaller. It was found that there is a critical temperature at which the intensity of the oxide phase is maximum, the intensity of the nitride phase is minimum and the sample has smallest grains. The results of corrosion tests showed that at this critical temperature, the corrosion current is higher and the corrosion resistance is lower. By simulating the equivalent, the reason for the maximum corrosion current at the critical temperature was investigated and attributed to the minimum electrical impedance (due to the minimum electrical resistance (reduction of Nitride phase), Large double layer capacitance (low oxide layer thickness compared to nitride layer thickness) and large coating capacitance (due to small grains)). As the temperature rises further than critical temperature, the oxide phase becomes unstable and the oxygen molecules leave the surface, and the conditions for nitride phase formation improve and the nitride phase intensity increases. Therefore, as the intensity of the nitride phase increases the electrical resistance increases and because of grain size increasing with temperature, the capacitance of the double layer and the capacitance of coating decrease. As a result, the corrosion resistance increases with increasing electrical impedance.

Acknowledgment
We would like to thank the university of Tehran and university of Mohaghegh Ardabili for their support.

Availability of data and materials
The data that support the findings of this study are available on request from the corresponding author.

Conflict of interests
The authors declare that they have no known competing financial interests or personal relationships that could have appeared to influence the work reported in this paper.

References

[1] L. L. Liu, P. X. Yang, C. N. Su, H. F. Guo, and M. Z. An. "Microstructure and corrosion behavior of micro-arc oxidation film on magnesium alloy.". *International Journal of Electrochemical Science*, **8**:6077–84, 2013.
DOI: https://doi.org/10.1016/S1452-3981(23)14742-0.

[2] F. Abdi. "Corrosion protection of AISI 304 stainless steel using thin films of manganese nitride.". *Journal of Applied Chemical Research.*, **15**:19–33, 2021.

[3] Y. Xin, C. Liu, W. Zhang, J. Jiang, G. Tang, X. Tian, and P. K. Chu. "Electrochemical behavior Al_2O_3/Al coated surgical AZ91 magnesium alloy in simulated body fluids.". *Journal of The Electrochemical Society*, **155**:C178, 2008.
DOI: https://doi.org/10.1149/1.2844433.

[4] C. S. Wu, Z. Zhang, F. H. Cao, L. J. Zhang, J. Q. Zhang, and C. N. Cao. "Study on the anodizing of AZ31 magnesium alloys in alkaline borate solutions.". *Applied Surface Science*, **253**:3893–8, 2007.
DOI: https://doi.org/10.1016/j.apsusc.2006.08.020.

[5] K. F. Khaled. "Studies of iron corrosion inhibition using chemical, electrochemical and computer simulation techniques.". *Electrochimica Acta*, **55**:6523–32, 2010.
DOI: https://doi.org/10.1016/j.electacta.2010.06.027.

[6] G. M. Spinks, A. J. Dominis, G. G. Wallace, and D. E. Tallman. "Electroactive conducting polymers for corrosion control: part 2. Ferrous metals.". *Journal of Solid State Electrochemistry*, **6**:85–100, 2002.
DOI: https://doi.org/10.1007/s100080100211.

[7] R. Racicot, R. Brown, and S. C. Yang. "Corrosion protection of aluminum alloys by double-strand polyaniline.". *Synthetic metals*, **85**:1263–4, 1997.
DOI: https://doi.org/10.1016/S0379-6779(97)80232-9.

[8] D. E. Tallman, Y. Q. Pae, and G. P. Bierwagen. "Conducting polymers and corrosion: Part 2 polyaniline on aluminum alloys.". *Corrosion*, **56**, 2000.
DOI: https://doi.org/10.5006/1.3280544.

[9] D. Huerta-Vilca, S. R. Moraes, and A. J. Motheo. "Electrosynthesized polyaniline for the corrosion protection of aluminum alloy 2024-T3. ". *Journal of the Brazilian Chemical Society*, **14**:52–8, 2003.
DOI: https://doi.org/10.1590/S0103-50532003000100009.

[10] N. A. Ogurtsov, A. A. Pud, P. Kamarchik, and G. S. Shapoval. "Corrosion inhibition of aluminum alloy in chloride mediums by undoped and doped forms of polyaniline.". *Synthetic Metals*, **143**:43–7, 2004.
DOI: https://doi.org/10.1016/j.synthmet.2003.10.015.

[11] R. Matero, M. Ritala, M. Leskelä, T. Salo, J. Aromaa, and O. Forsén. "Atomic layer deposited thin films for corrosion protection.". *Le Journal de Physique IV*, **9**:Pr8–493, 1999.
DOI: https://doi.org/10.1051/jp4:1999862.

[12] W. T. Ting, K. S. Chen, and M. J. Wang. "Dense and anti-corrosion thin films prepared by plasma polymerization of hexamethyldisilazane for applications in metallic implants.". *Surface and Coatings Technology*, **410**:126932, 2021.
DOI: https://doi.org/10.1016/j.surfcoat.2021.126932.

[13] M. A. Fusco, Y. Ay, A. H. Casey, M. A. Bourham, and A. L. Winfrey. "Corrosion of single layer thin film protective coatings on steel substrates for high level waste containers.". *Progress in Nuclear Energy*, **89**:159–69, 2016.
DOI: https://doi.org/10.1016/j.pnucene.2016.02.016.

[14] J. F. Flores, S. B. Valdez, M. Schorr, and J. J. Olaya. "Corrosion protection of steels by PVD TaN thin films.". *Anti-Corrosion Methods and Materials*, **53**:88–94, 2006.
DOI: https://doi.org/10.1108/00035590610650785.

[15] W. Ensinger, O. Lensch, J. Knecht, K. Volz, T. Matsutani, and M. Kiuchi. "Pitting corrosion of aluminum coated by ion beam assisted deposition of carbon with argon ions at different ion-to-atom arrival ratios.". *Surface and Coatings Technology*, **158**:594–8, 2002.
DOI: https://doi.org/10.1016/S0257-8972(02)00315-8.

[16] Y. Massiani, J. P. Crousier, L. Fedrizzi, S. Gialanella, and P. L. Bonora. "Electrochemical study of multiple-energy nitrogen-ion-implanted aluminium alloys.". *Materials Science and Engineering: A*, **116**:53–7, 1989.
DOI: https://doi.org/10.1016/0921-5093(89)90127-5.

[17] W. S. Tait, C. O. Huber, B. C. Begnoche, J. R. Siettmann, and C. R. Aita. "Al, Al–N alloy, and AlN-coated steel corrosion behavior in O_2-free KCl solutions.". *Journal of Vacuum Science & Technology A: Vacuum, Surfaces, and Films*, **6**:924–7, 1988.
DOI: https://doi.org/10.1116/1.575031.

[18] S. Venkatraman, M. R. Nair, D. C. Kothari, K. B. Lal, and R. Raman. "Anodic polarization behaviour of ion implanted aluminum in 3.5 wt.% NaCl electrolyte.". *Nuclear Instruments and Methods in Physics Research Section B: Beam Interactions with Materials and Atoms*, **19**:241–6, 1987.
DOI: https://doi.org/10.1016/S0168-583X(87)80051-4.

[19] L. Zhang, J. H. Booske, and J. L. Shohet. "Anti-corrosive surface modification of 6061 aluminum using plasma source ion implantation.". *Materials Letters*, **22**:29–33, 1995.
DOI: https://doi.org/10.1016/0167-577X(94)00215-0.

[20] J. H. Booske, L. Zhang, W. Wang, K. Mente, N. Zjaba, C. Baum, and J. L. Shohet. "Nitrogen plasma source ion implantation for corrosion protection of aluminum 6061-T4.". *Journal of Materials Research*, **12**:1356–66, 1997.
DOI: https://doi.org/10.1557/JMR.1997.0185.

[21] Y. K. Shim, Y. K. Kim, K. H. Lee, and S. Han. "The properties of AlN prepared by plasma nitriding and plasma source ion implantation techniques.". *Surface and Coatings Technology*, **131**:345–9, 2000.
DOI: https://doi.org/10.1016/S0257-8972(00)00807-0.

[22] D. Priyantoro, E. Mulyani, and T. Sujitno. "Effect of nitrogen ion implantation on the surface hardness, corrosion rate, and crystal structure of pure aluminium.". *Adv Mater*, **8**:137, 2019.
DOI: https://doi.org/10.11648/j.am.20190804.12.

[23] E. A. Starke Jr and J. T. Staley. "Application of modern aluminum alloys to aircraft. ". *Progress in Aerospace Sciences*, **32**:131–72, 1996.
DOI: https://doi.org/10.1016/0376-0421(95)00004-6.

[24] Q. Li, J. O. Jensen, and N. Bjerrum. "Chemistry, electrochemistry, and electrochemical applications: Aluminum.". *InEncyclopedia of Electrochemical Power Sources*, pages 695–708, 2009.
DOI: https://doi.org/10.1016/B978-044452745-5.00951-5.

[25] W. S. Tait. "Corrosion prevention and control of chemical processing equipment. InHandbook of environmental degradation of materials.". *William Andrew Publishing*, pages 565–581, 2005.
DOI: https://doi.org/10.1016/B978-1-4377-3455-3.00028-6.

[26] F. Fateme and H. Savaloni. "Methane conversion by repetitive nanosecond pulsed plasma.". *Transactions of Nonferrous Metals Society of China*, **27**:701–10, 2017.
DOI: https://doi.org/10.1016/S1003-6326(17)60078-5.

[27] F. Abdi and H. Savaloni. "Influence of N^+ ion implantation at different temperatures on nanostructural modifications and characteristics of Al alloy surface.". *Philosophical Magazine*, **96**:1305–17, 2016.
DOI: https://doi.org/10.1080/14786435.2016.1162912.

[28] H. Savaloni and F. Modiri. "Surface nano-structural modifications and characteristics in nitrogen ion implanted W as a function of temperature and N^+ energy.". *Applied Surface Science*, **253**:1135–42, 2006.
DOI: https://doi.org/10.1016/j.apsusc.2006.01.066.